## 5. Supplementary Data

### *5.1. Measurement of normal growth*

The embryonic BT steadily bends and grows during the stages following initial sulcus formation. To quantify regional growth over the course of development, we measured regional BT dimensions from stages HH11 to HH20 using OCT (Fig. S1). By tracing the perimeter of the inner wall over the course of development (Fig. S1A–B, n=6–9 embryos per group), we saw that average vesicle radii (T, D, M) increase approximately linearly with hours of development. The rate of radius increase was highest for the telencephalon-hypothalamus complex ($\dot{r}_T$ = 0.012 mm/h, $R_T$(40h) = 0.14 ± 0.02 mm), followed by the midbrain ($\dot{r}_M$ = 0.010 mm/h, $R_M$(40h) = 0.11 ± 0.02mm), and lastly the diencephalon ($\dot{r}_D$ = 0.008 mm/h, $R_D$(40h) = 0.12 ± 0.01mm). Linear correlation was highest for the midbrain region (Fig. S1C, $R^2$ = 0.95), and for this reason the midbrain radius was used to compare growth models in subsequent analysis.

Regional thickness was also estimated at HH11 (n=10) and HH17-18 (n=8). To obtain a single value for each cross section, average wall thickness was estimated as the wall area (bounded by outer and inner edges) divided by perimeter. We observe insignificant thickening of the forebrain regions (Fig. S1D) but significant thickening of the midbrain (P<0.001), which could result in part from bending. Note that this increase is less than 40%, while circumference increases by 240% across the same stages.

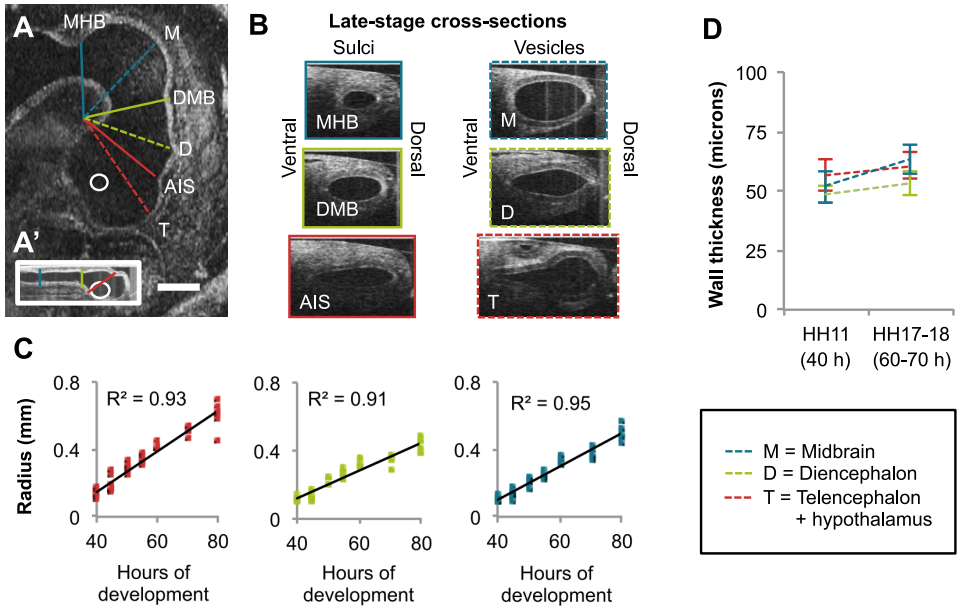


Figure S1: Change in lumen size during development. (**A**) Sagittal OCT cross section of HH17 brain tube. Dashed lines cross through the middle of each vesicle, solid lines cross through sulci. (**A**) For comparison, sagittal cross section of a HH12 brain tube is shown to scale. (**B**) Sulci and vesicle cross sections corresponding to each line in A. (**C**) Average vesicle radius (perimeter/$2\pi$) versus time of development (HH11–20). (**D**) Average vesicle wall thickness (wall area/perimeter) at HH11 and HH17. T=telencephalon, D=diencephalon, M=midbrain, AIS=anterior intraencephalic sulcus, DMB=diencephalon-midbrain boundary sulcus, MHB=midbrain-hindbrain boundary sulcus, overlaid circle in A, A' denotes location of optic stalk. Scale bar: 0.5 mm, all images shown to scale.

*5.2. Experiments to rule out external factors*

Several potential mechanisms of forebrain morphogenesis were ruled out through experiments. To consider contractile response at a shorter time scale, ATP was applied to permeabilized embryos at HH12 (n=5). To rule out effects of the surrounding mesenchyme, several brain tubes were isolated and cultured in control media (n=3) or media containing calyculin A (n=5). Results in Fig. S2A–C indicate that contraction is intrinsic to the neuroepithelium.

Upon extraction from the egg, we observed that brain tubes had failed to close in several embryos (n=3), producing exencephaly (open brain tube). The AIS, DMB, and MHB were still constricted in all cases, suggesting that pressure is not necessary for initial sulcus formation (Fig. S2D). Furthermore, Nile blue stain did not indicate patterned cell death in vesicles or sulci (n=10 HH11–13 and n=11 HH16–18, Fig. S2E). Late-stage embryos (HH14–17) were also cultured for 6 h in 30nM (n=6) or 100nM (n=5) calyculin A (Fig. S2F–F"). No effect was observed, but confocal imaging revealed that F-actin was still present on the apical surface of sulci and vesicles at late stages (n=14 HH16–18, Fig. S2G). These results suggest that actin structure remains intact but actomyosin contraction has little effect on BT shape at later stages.

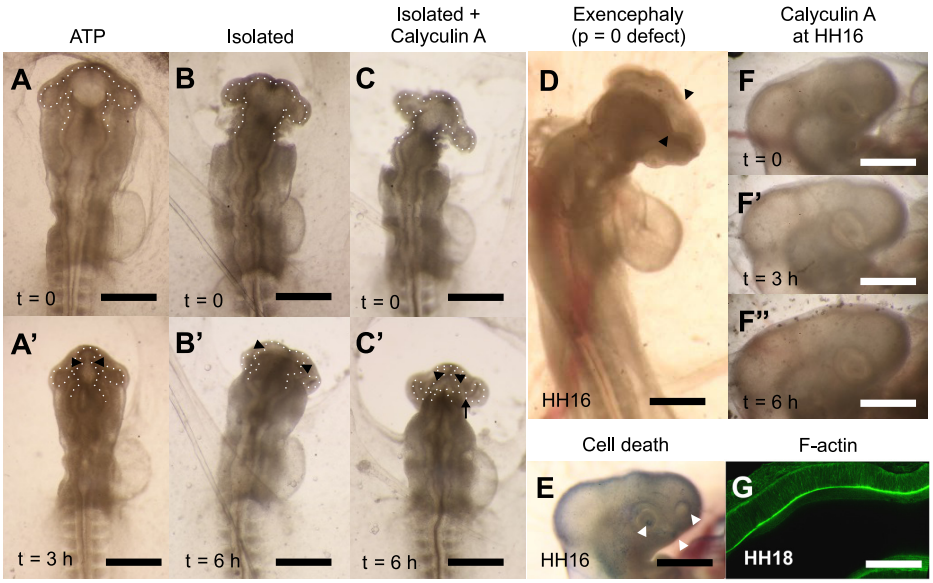


Figure S2: Experiments to rule out external factors. (**A–A'**) Application of ATP produced hypercontraction after 3 h, similar to embryos cultured in calyculin A. (**B–B'**) Removing external mesenchyme and membranes to isolate embryos (HH11–12) caused slight hypercontraction after 6 h culture in control media. (**C–C'**) However, those isolated and cultured 6 h in calyculin A exhibited strong hypercontraction (n=5), similar to non-isolated embryos. (**D**) In embryos for which the neural tube failed to close (during development in ovo), constrictions were still observed between all vesicles. (**E**) Staining for cell death (Nile blue) did not indicate cell death at brain sulci. White arrowheads indicate locations where stain is positive for cell death: lens, otic placode, and optic fissure. (**F–F"**) When embryos were cultured in calyculin A beyond HH14, no effect was observed, suggesting actomyosin contraction has relatively little effect on BT morphology at these stages. (**G**) F-actin remains concentrated on the apical surface of sulci and vesicles at late stages. Scale bars on brightfield images are 500 $\mu$m; scale bar on confocal image is 200 $\mu$m. Black arrowheads indicate AIS; black arrow points to maximally hyperconstricted optic stalk.

### 5.3. *Model parameters*

| Dimension | Source | Measured Value | Model Value | Figure |
|---|---|---|---|---|
| $R$ | OCT ($R_M$) | 0.11 ± 0.02 mm | 0.1 mm | 4A (top) |
| $L$ | OCT | 0.46 ± 0.02 mm | 0.5 mm | 4A (top) |
| $R_T$ | OCT | 0.14 ± 0.02 mm | 0.15 mm | 4A (bottom) |
| $R_{OV}$ | OCT | 0.06 ± 0.01 mm | 0.08 mm | 4A (bottom) |
| $W$ | OCT | 0.56 ± 0.07 mm | 0.06 mm | 4A (bottom) |
| $h$ | OCT | 54 ± 5 $\mu$m | 50 $\mu$m | 4A |
| $^*X_{OS}$ | Confocal | 0.20 mm | 0.20 mm | 4C, 6 |
| $^*Z_{DMB}$ | Confocal | 0.13 mm | 0.13 mm | 4C, 6 |
| $^*Z_{AIS}$ | Confocal | 0.38 mm | 0.38 mm | 4C, 6 |

Table S1: Model dimensions and sources. All OCT dimensions were measured at HH11. Items marked with * denote peaks of $S_\Theta/S_Z$, which were not measured until HH12. For the BT model, the spacing between constrictions was adjusted to a total length $L$ to account for longitudinal growth from HH11 to HH12. For the SP model, $W$ did not change substantially from HH11 to HH12.

| Parameter | Source | Model Value | Equation |
|---|---|---|---|
| $\psi_{iso}$ | Confocal (Fig. 3A"-C") | 0.5 | Eq. 5, 6 |
| $\psi_\Theta, \psi_Z$ | $S_\Theta, S_Z$ (Eq. 1, Fig. 3, 4C) | Eq. 11 | Eq. 5, 6 |
| $\mu$ | Xu et al. (2010) | 200 Pa | Eq. 7 |
| $\kappa$ | Xu et al. (2010) | 20,000 Pa | Eq. 7 |
| $\mu_\Theta, \mu_Z$ | $S_\Theta, S_Z$ (Eq. 1, Fig. 3, 4C) | Eq. 10 | Eq. 7 |
| $C$ (normal) | Nakajima and Tanoue (2010) | 0.5 | Eq. 8 |
| $C$ (hyper) | $\lambda_{\Theta,D}$ | 0.3 | Eq. 8 |
| $\alpha$ | free parameter | 4 | Eq. 10 |
| $g_0$ | $G_0$ | 0.02 $h^{-1}$ | Eq. 12 |
| $g_\sigma$ | $G/G_0$ | $5g_0$ | Eq. 12 |
| $(\frac{\mu_N}{\mu})_{max}$ | Adams et al. (1990); Agero et al. (2010) | 100 | $\frac{\mu_N}{\mu} = 100e^{\frac{-10(Y+R+h)}{(R+h)}}$ |

Table S2: Model parameters and sources. With the exception of one free parameter, $\alpha$, all parameters were taken from literature or calculated/calibrated from experimental measurements.

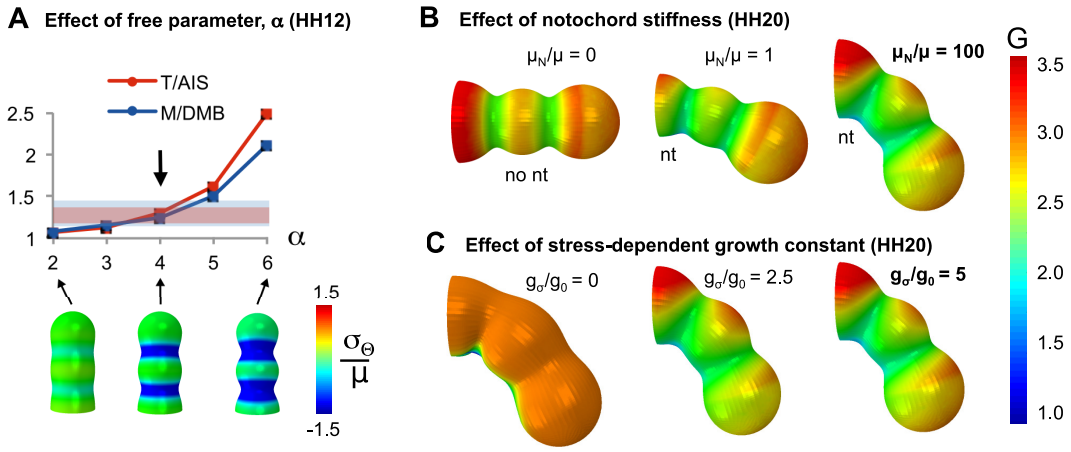


Figure S3: Effects of free parameter ($\alpha$), notochord, and stress-dependent growth on final BT shape. (**A**) As contraction parameter $\alpha$ increases (see Eq. 10), actin stiffness and relative sulcal depth increase. Red box represents the range of T/AIS and blue box represents range of M/DMB measured experimentally at HH12 (mean ± standard deviation). For the control case (C=0.5), $\alpha$ = 4 (arrow) produces T/AIS and M/DMB within the correct ranges. (**B**) Bending increases as notochord (nt) modulus $\mu_N$ increases. (**C**) As the stress-dependent growth rate parameter ($g_\sigma$) increases relative to the constant growth rate parameter ($g_0$), sulci become more distinct. Final model values for (B–C), based on measurement or calibration, are shown in bold.

### 5.4. *Notochord cutting experiments*

In our computational models that include cephalic flexure, the growing brain tube is constrained by a nongrowing notochord along the ventral midline. This quickly builds longitudinal tension in the notochord as it resists growth of the surrounding tissue (Fig. S4A). To test whether this occurs in the embryo, the BT was isolated in embryos after the onset of bending (HH12–13, n=6) and the notochord was surgically cut. In all cases, the notochord sprang apart (Fig. S4B), suggesting that it is in tension.

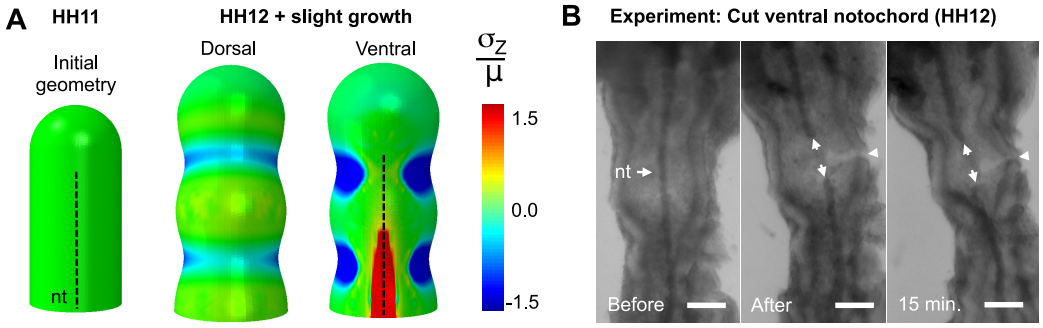


Figure S4: Notochord tension supports constrained growth model of flexure. (**A**) When the BT model including ventral notochord (nt) is allowed to grow, longitudinal tension develops in the nongrowing notochord (HH12+). At early stages, dorsal and lateral regions are still under compression or near-zero longitudinal stress. (**B**) When the notochord is cut at similar stages, it springs apart suggesting tension (white arrows). Alternately, a cut in the lateral BT shows minimal change, suggesting relatively low stress (white arrowhead). Scale bars: 100 $\mu$m. Experimental images courtesy of Dr. Benjamen Filas.

### 5.5. *Measurement of normal pressure*

Embryonic CSF pressure was recorded using a servo-null micropressure system (model 5A, Instruments for Physiology and Medicine, San Diego, CA) as described by Chabert and Taber (2002). To measure pressure in the early brain tube (HH12–13), pipette tips were inserted into the midbrain. Pressure measurements shown in Fig. S5 fall within the range measured by Jelinek and Pexieder (1968).

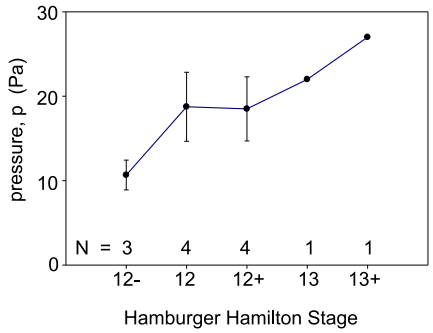


Figure S5: Lumen pressure measurements in vivo (mean ± standard deviation). Data courtesy of Dr. Shuddahadeb Ray.

**Reference:** Chabert S. and Taber L.A., Intramyocardial pressure measurements in the stage 18 embryonic chick heart, Am. J. Physiol.-Heart Circ. Physiol. **282** (4), 2002, H1248H1254.

*5.6. Optic vesicles have minimal effect on overall brain tube (BT) morphogenesis*

After initial contraction, the optic vesicles and optic stalks undergo complex morphogenesis that is outside the scope of this paper. To determine whether optic vesicles had an effect on the behavior of the BT at later stages, optic vesicles were surgically removed at the stalk (HH11–13), and the embryos were cultured for 18–24 h on a 0.3% agarose albumin gel as described by Chapman et al. (2001) for improved viability. After healing, the BT retained normal development with respect to the AIS and DMB (Fig. S6). In fact, the hypothalamus was less compressed in these embryos (T more circular) and more closely resembled the shape of our model.

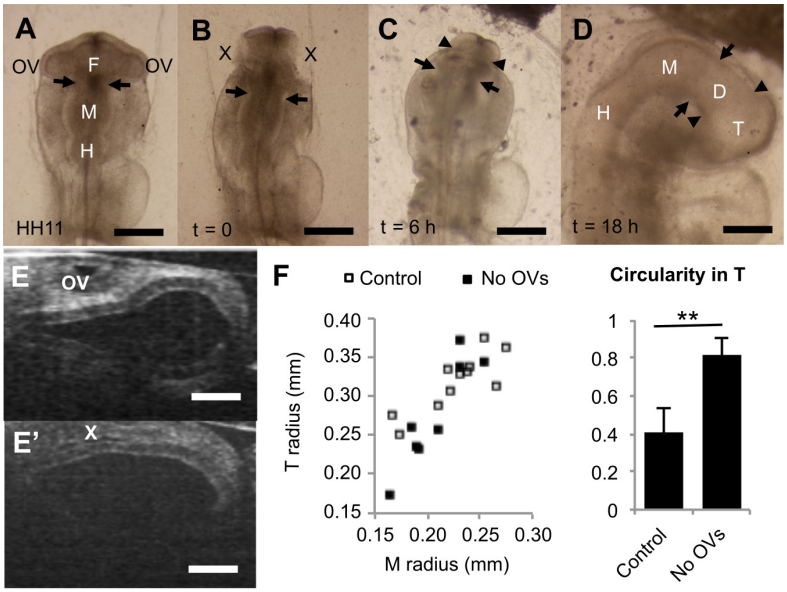


Figure S6: Removal of OVs has minimal effect on late stage BT morphogenesis. (**A–D**) Representative bright field images comparing embryo before perturbation (A), after OV removal (B), after wound healing and AIS formation (C), and after BT expansion and bending (D, shown at HH15). (**E**) Representative OCT cross section of control telencephalon-hypothalamus complex (T) at HH17. (**E'**) Representative OCT cross section of T at HH17 for embryos in which OVs had been surgically removed. (**F**) Left: scatterplot of T radii versus midbrain (M) radii (HH15–17) for control (n=11, black) and experimental (n=8, white) embryos. Midbrain radius was chosen as the x-axis because it offered the closest linear correlation with stage (Fig. S1). Right: Circularity of the lumen was significantly higher in T when the OVs were removed. A value of 1 corresponds to a perfect circle, similar to the circular cross section assumed in BT models. Scale bars: 300 $\mu$m for (A–D), 200 $\mu$m for (E). ** denotes P<0.001, X denotes absent OV.